Journal of Intelligent Systems and Internet of Things
Vol. 17, No. 02, PP. 119-132, 2025
DOI: https://doi.org/10.54216/JISIoT.170209

Computational Artificial Neural Network Performances for the Fractional Order Lumpy Skin Disease Model

Saleh Ali Alomari[1,*]
[1]Computer Science Department, Faculty of Information Technology, Jadara University, Irbid 21110, Jordan
Email: omari08@jadara.edu.jo

Abstract

The motive of current investigations is to design a computational artificial neural network procedure for the numerical outputs of the fractional order (FO) lumpy skin disease model (LSDM), called as FO-LSDM. The stochastic performances using the optimization of scale conjugate gradient (SCGD) have been implemented to get the solutions of the FO-LSDM. The aim to implement the solutions of the FO is considered more reliable as compared to the integer order. The mathematical form of the LSDM is divided into two populations based on the cattle and vector using the population of susceptible and infected. A numerical Adam scheme is plagued to accomplish the dataset for reducing the mean square error by splitting the statics of endorsement, testing and training as 13%, 12% and 75%. The proposed stochastic neural network approach has a single layer, thirty numbers of neurons, sigmoid activation function, and optimization based SCGD procedure. The exactitude of the SCGD neural network is authenticated through the result comparisons and reducible absolute error around 10-06 to 10-08. Additionally, the correctness of the stochastic process based on the SCGD neural network is evaluated by applying the procedure of state transitions, correlation values, and best training.

Received: January 01, 2025 Revised: March 01, 2025 Accepted: May 24, 2025

Keywords: Fractional order; Lumpy skin disease; Mathematical model; Scale conjugate; Artificial Neural network

1. Introduction

Over the past few centuries, implementations of mathematics have gained importance in a variety of fields for understanding and addressing complex problems. It is useful as a powerful tool for applying numerous theorems to describe and assess the motions of operations. In many fields, including social sciences, biology, economics, physics, and engineering, mathematical mechanisms are used to represent real issues in an organized way using various principles and languages. Several mathematical frameworks are predictable, depending on predictable processes that are straightforward. The Kepler computations and a few other corresponding problems are simulated using this well-known motion law that Newton proposed, within which the future status of the system is resolved precisely in its current form. This is very important for comprehending the circular conduct linked to essential forces [1]. Several of the mathematical equations are stochastic, meaning that unpredictability and instability are incorporated. Another instance is the stochastic systems-based valuation simulation, which used random market fluctuations to predict price trends. Additionally, Onder et al. [2] produced the surprising optic responses by mimicking the modified Schrödinger theory with the principle of Kerr adopting the framework of Ito calculus in the discipline of optical science. Alquran et al. [3] have published the results of the Kadomtsev–Petviashvili framework taking into account second-order spatial and periodic longitudinal dispersion impacts. These investigations can be used to simulate ion-acoustic sounds in plasma dynamics and vibrations in shallow oceans, among other applications. Several structures that benefit from computational modelling are listed in the sources [4]. In epidemiology, computer modelling is crucial for understanding and predicting the evolving trends of various diseases because of its ability to identify underlying factors and provide measures to prevent them. The

transmission of the monkeypox virus, for instance, and its prevention measures have been studied in [5]. As another example, because the illness's 2019 introduction, coronavirus assessment has grown into an extensive area of research as researchers try to understand how it functions. Joshi et al. [6] investigated the mathematical modelling and equilibrium assessment of a fractional type of non-singular coronavirus, taking into account unpredictable incidence and repair frequencies. Joshi et al.'s study [7] examined the fractional sort of coronavirus framework, comparing the results with real statistics from India and evaluating the effect of vaccination on its capacity to spread. These variables are just a small sample of the excellent work being done in coronavirus prediction. Some of the common virus strains includes Lassa [8], dengue [9], TB [10], and Ebola [11]. These diseases not only damage humans but also propagate across other organisms, such as cattle, and have a terrible effect on the calorie content of meals. Among many illnesses that cattle might get, lumpy skin (LS) is one that is a specific harmful disease. This highly transmissible illness mostly affects cattle in developing nations such as Africa and Asia. These nations are particularly vulnerable economically as their economies rely heavily on food production, making them particularly vulnerable to an illness that causes LS. This disease associated with the Capripox virus group causes it. The disorder that results in clusters or lumps growing on the topmost layer of those impacted is referred to as LS. Moreover, cattle having LS are highly contagious and can spread fast through contaminated tools, direct touch, and transmission of insects. A collection of animals that contracts a sickness could see significant declines in milk production. Low fertility and early pregnancies cause manufacturers to incur significant economic losses. Moreover, the disease results in chronic harm to bovine conceals, lowering the livestock's market value. Because of the drug's serious adverse reactions, LS has been classified by the international society for veterinary medicine as an illness requiring to be promptly notified. Owners are required by law to disclose any potential employing of LS within a specified period. By mandating surveillance, authorities may swiftly implement measures to halt its spread and mitigate its impact on the livestock sector. The condition of LS has been inhibited in livestock to prevent the infection from propagating. In such management initiatives, safeguards and wellness techniques are typically employed. Vaccination is a key technique to prevent LS, and many vaccines have been developed to increase vaccination against the sickness in those affected. Vaccination programs are intended to protect vulnerable animals and prevent the disease from transmitting among groups of animals. Tight hygiene practices have been shown to be necessary to stop the LS virus from spreading, and this may serve as a further weapon in the campaign over the infection. Putting in place procedures for cleaning structures as well as equipment is essential for reducing the risk of spreading viruses. By employing pesticides and creating architecture, which is resistant to organisms, insect control methods can minimize the number of vector species. In addition, constant surveillance systems are necessary for the early detection of LS outbreaks.

By employing insect control methods such as applying pesticides and creating impermeable lodging, the number of transmitting insects may be minimized. Moreover, continuous surveillance systems are necessary for the early detection of LS outbreaks. LS has become more common elsewhere than in Africa in recent years. Pandemics have been reported in countries throughout Asia, Europe, and the Middle East. In current decades, reports of LS have been made in Greece, Serbia, North Macedonia, Albania, and Bulgaria. Asia-wide, LS has been reported in Iran, Turkey, India, and Pakistan. Furthermore, the countries where the sickness has been discovered are Iraq, Jordan, and Saudi Arabia. It is clear that the proportion of infected livestock has grown throughout time and then decreased when the immunization program was initiated. Moreover, other factors that have been linked to the worldwide spread of LS include international trade, animal travel that carries the virus, and the presence of mosquitoes that can spread the disease. Increased migration and industry across the regions, together with the rise of the cattle sector, have been linked to the development of LS in new places.

The current investigations provide a computational Artificial Neural Network (ANN) procedure using the optimization of scale conjugate gradient (SCGD) for the numerical outputs of the fractional order (FO) lumpy skin disease model (LSDM), i.e., FO-LSDM. The stochastic performances based on the ANN have been oppressed in the various presentations, e.g., delay differential models, fractional order systems, and virus spreading frameworks. The researchers have taken keen interest to present the numerical results of the LSDM using the process of ANN along with SCGD in light of these applications. The mathematical LSDM is divided into two populations based on the cattle and vector using the population of susceptible and infected at time u, shown as [12-18]:

$$\begin{cases} D^{\kappa} S_c(u) = \Lambda_c - \left[\alpha_c I_c(u) + \gamma_c + \beta_c I_v(u)\right] S_c(u), & S_c(0) = i_1, \\ D^{\kappa} I_c(u) = \left[\alpha_c S_c(u) - (\gamma_c + \delta_c)\right] I_c(u), & I_c(0) = i_2, \\ D^{\kappa} S_v(u) = \Lambda_v - \left[\gamma_v + \alpha_v I_v(x)\right] S_v(u), & S_v(0) = i_3, \\ D^{\kappa} I_v(u) = \left[\alpha_v S_v(u) - (\gamma_v + \delta_v)\right] I_v(u), & I_v(0) = i_4, \end{cases} \tag{1}$$

4

Where κ is the fractional order Caputo derivative, α_c signifies the infection rate in susceptible animals based infected cattle, Λ_c is the cattle growth rate, γ_c represents natural death rate of animals, β_c presents the infection rate in susceptible animals populations of infected vectors, Λ_v denotes the reproduction rate of vectors, δ_c indicates the animals death ratio based on the infection, α_v presents the infection ratio in susceptible population, δ_v is the death rate in infected vectors, and γ_v describe the natural death in vectors, while *i*1, *i*2, *i*3 and *i*4 are the initial conditions (ICs). Some novel points of this study are discussed as:

- A novel procedure based on the ANN procedure using the optimization of SCGD is presented successfully for the numerical outputs of the FO-LSDM.
- The proposed stochastic ANN approach has been applied with a single layer using the sigmoid activation function.
- The fractional order derivatives in the ranges of 0 and 1 have been used first time to solve the LSDM.
- Thirty numbers of neurons have been used in this stochastic process, while the optimization is performed by using the SCGD procedure.
- The exactness of the ANN procedure using the SCGD optimization is authenticated by using the reducible absolute error (AE), results overlapping, and regression coefficient values for solving each case of the system.

The other paper is organized as: The description of the mathematical procedure is shown in Section 2, the numerical outputs of the LSDM are provided in Section 3, whereas the concluding remarks are derived in the final Section.

2. Methodology

This section represents the ANN procedure using the optimization of SCGD in order to solve the nonlinear LSDM.

2.1 SCGD scheme

The proposed SCGD optimizing scheme is developed during ANN to avoid the problem of overfitting. It achieves it by changing the framework's weights based on previous expertise acquired through learning. One of the objectives of training for the traditional neural network is to reduce the mean square error (MSE), which is based on actual objectives and anticipated results. The algorithm based on SCGD is one of the optimization techniques, which is applied to reduce the cost function in machine learning systems. The initialization is performed through the scaling factor and system's parameters. Calculate the direction of conjugate gradient (CG) by applying the updated parameters as well as loss function gradient. The direction of CG is scaled by using the process of scaling factor. A line search is performed to calculate the optimal values of the step size. The system's parameters are update by applying the direction of SCGD along with the best step size. The advantages of SCGD are improved stability, faster convergence, and robustness. However, the common applications of SCGD are neural networks, deep learning, and regression systems. Fig. 1 shows a SCGD technique including layer constructions, numerical outputs, and conceptual proposals. The designed methodology presents the solutions of the nonlinear FO-LSDM by taking a single hidden layer, thirty numbers of neurons, sigmoid activation function, tolerance 10^{-08}, and 0.01 step size.

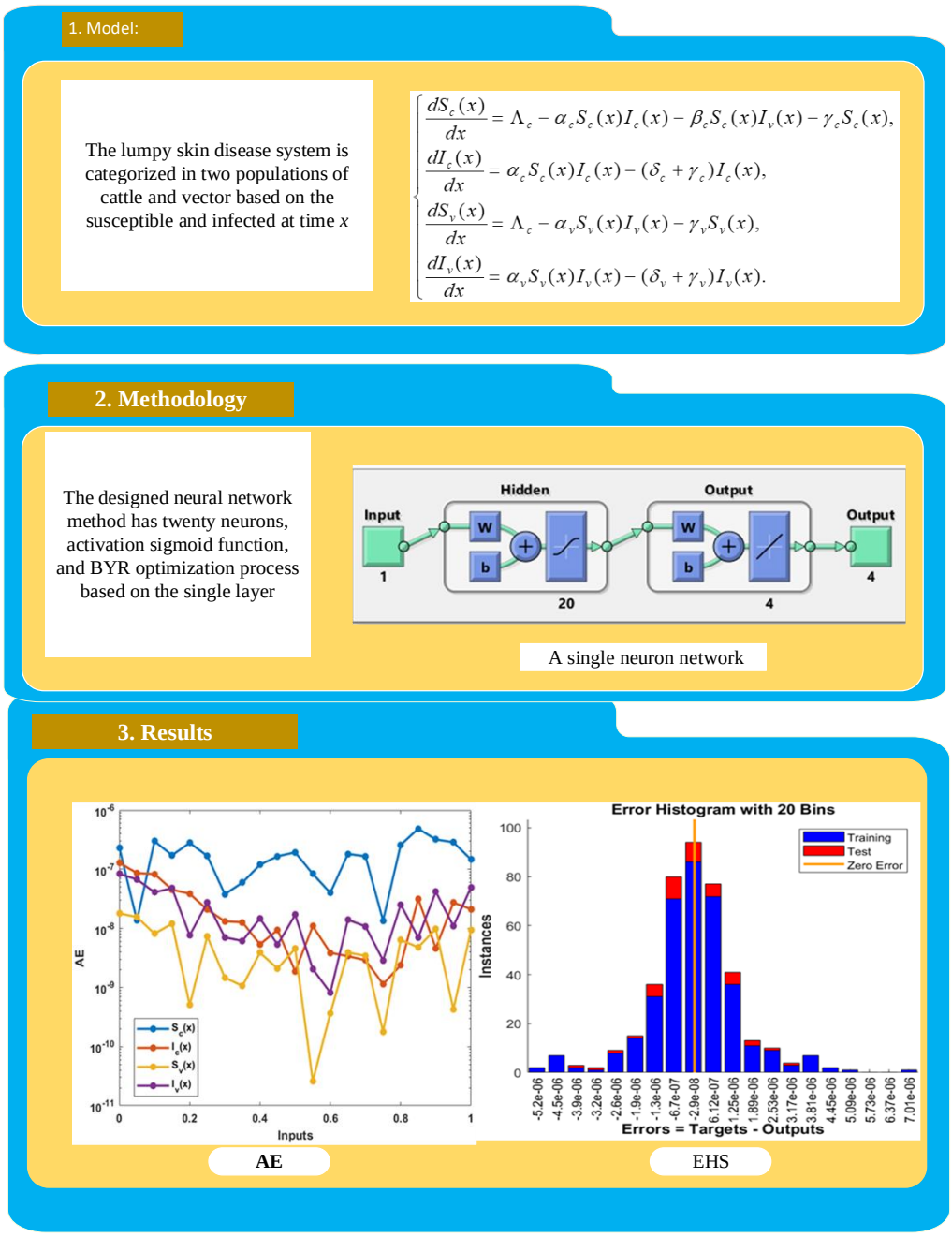

Figure 1. Workflow diagram of the nonlinear FO-LSDM

It is performed that the optimization of SCGD in order to solve the nonlinear FO-LSDM by taking thirty neurons, which have the optimal demonstrations in the framework of overfitting or underfitting situations. It has been discovered that shorter neurons can achieve the parameter-related convergence; nevertheless, this increases the likelihood of rapid convergence. While using further neurons can yield incredibly precise outcomes, it can also result in excessive fitting. Thirty neurons have been designated and statics of training, endorsement and testing is selected for endorsement, testing and training as 13%, 12% and 75%. Although using more neurons can produce incredibly precise outcomes that perform the overfitting outputs. Fifty percent of the information is used to conduct assessments and authorization, whereas the other fifteen percent is used for training. Fig. 2 demonstrates the layer design used in the nonlinear FO-LSDM framework simulations.

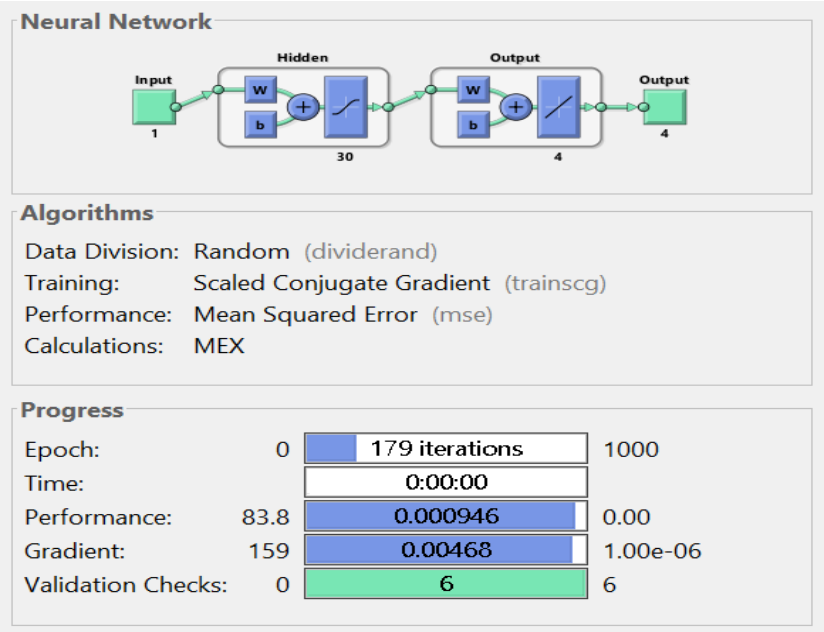

Figure 2. A layer construction for the nonlinear FO-LSDM

3. Numerical solutions of the nonlinear FO-LSDM

In this section, the numerical performances of the nonlinear FO-LSDM are available by selecting the suitable parameters in three cases, which is shown as:

Case 1: Consider $\kappa = 0.5$, $\Lambda_c = 4$, $\alpha_c = 0.1$, $\beta_c = 0.59$, $\gamma_c = 0.6$, $\delta_c = 0.3$, $\Lambda_v = 0.055$, $\alpha_v = 0.2$, $\gamma_v = 0.3$, $\delta_v = 0.2$, whereas the ICs are 0.1, 0.2, 0.3 and 0.4.

$$\begin{cases} D^{0.5}S_c(u) = 4 - [0.1I_c(u) - 0.59I_v(u) - 0.6]S_c(u), & S_c(0) = 0.1, \\ D^{0.5}I_c(u) = [0.1S_c(u) - 0.9]I_c(u), & I_c(0) = 0.2, \\ D^{0.5}S_v(u) = 0.055 - [0.2I_v(u) + 0.3]S_v(u), & S_v(t) = 0.3, \\ D^{0.5}I_v(u) = [0.2S_v(u) - 0.5]I_v(u), & I_v(0) = 0.4. \end{cases} \tag{2}$$

Case 2: Consider $\kappa = 0.7$, $\Lambda_c = 4$, $\alpha_c = 0.1$, $\beta_c = 0.59$, $\gamma_c = 0.6$, $\delta_c = 0.3$, $\Lambda_v = 0.055$, $\alpha_v = 0.2$, $\gamma_v = 0.3$, $\delta_v = 0.2$, whereas the ICs are 0.1, 0.2, 0.3 and 0.4.

$$\begin{cases} D^{0.7}S_c(u) = 4 - [0.1I_c(u) - 0.59I_v(u) - 0.6]S_c(u), & S_c(0) = 0.1, \\ D^{0.7}I_c(u) = [0.1S_c(u) - 0.9]I_c(u), & I_c(0) = 0.2, \\ D^{0.7}S_v(u) = 0.055 - [0.2I_v(u) + 0.3]S_v(u), & S_v(t) = 0.3, \\ D^{0.7}I_v(u) = [0.2S_v(u) - 0.5]I_v(u), & I_v(0) = 0.4. \end{cases} \tag{3}$$

Case 3: Consider $\kappa = 0.9$, $\Lambda_c = 4$, $\alpha_c = 0.1$, $\beta_c = 0.59$, $\gamma_c = 0.6$, $\delta_c = 0.3$, $\Lambda_v = 0.055$, $\alpha_v = 0.2$, $\gamma_v = 0.3$, $\delta_v = 0.2$, whereas the ICs are 0.1, 0.2, 0.3 and 0.4.

$$\begin{cases} D^{0.9}S_c(u) = 4 - [0.1I_c(u) - 0.59I_v(u) - 0.6]S_c(u), & S_c(0) = 0.1, \\ D^{0.9}I_c(u) = [0.1S_c(u) - 0.9]I_c(u), & I_c(0) = 0.2, \\ D^{0.9}S_v(u) = 0.055 - [0.2I_v(u) + 0.3]S_v(u), & S_v(t) = 0.3, \\ D^{0.9}I_v(u) = [0.2S_v(u) - 0.5]I_v(u), & I_v(0) = 0.4. \end{cases} \tag{4}$$

The numerical performances of the FO-LSDM using the optimization of SCGD are displayed in Figs. 3 to 7. The MSE outputs and transition state (TS) are presented in Fig. 4(a to c). It demonstrates how training and evaluation processes are being used to check the acquired MSE. These obtained performances are signified as 1.52818×10^{-03}, 5.10060×10^{-03} and 1.95083×10^{-03} at iterations 179, 59 and 121 for each case of the FO-SCGD. The gradient presentations based on assessments are displayed in Figs. 3(d to f) that are shown as 4.6758×10^{-03}, 4.9669×10^{-02}, and 1.0429×10^{-02} for the FO-LSDM. The gradient depiction and these optimal results approve the precision of the SCGD process. The standards of the fitness function derived from the results are depicted in Fig. 4(a to c). The statistics based on the error histogram (EH) using the FO-LSDM are calculated in Fig. 4(d to f) that are shown as 5.391×10^{-03}, 8.8936×10^{-03}, and 2.930×10^{-04}. Figs. 5 to 7 present the correlation curves that show the regression coefficient levels reported as 1 for each case of the FO-LSDM. Table 1 presents the training data also with the statics of testing and authorization for solving the FO-LSDM.

Table 1: Optimal training values for solving the FO-LSDM

Case	M.S.E			Performance	Gradient	Epoch
	Training	Substantiation	Testing			
1	9.54072×10^{-04}	1.52818×10^{-03}	8.31985×10^{-04}	9.46×10^{-04}	4.68×10^{-03}	179
2	4.44312×10^{-03}	5.10060×10^{-03}	5.68471×10^{-03}	4.13×10^{-03}	4.97×10^{-02}	59
3	1.34792×10^{-03}	1.95083×10^{-03}	1.51176×10^{-03}	1.20×10^{-03}	1.04×10^{-02}	121

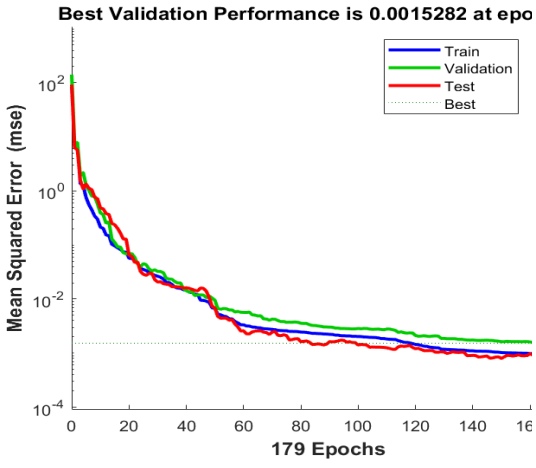

(a) Optimal training (1)

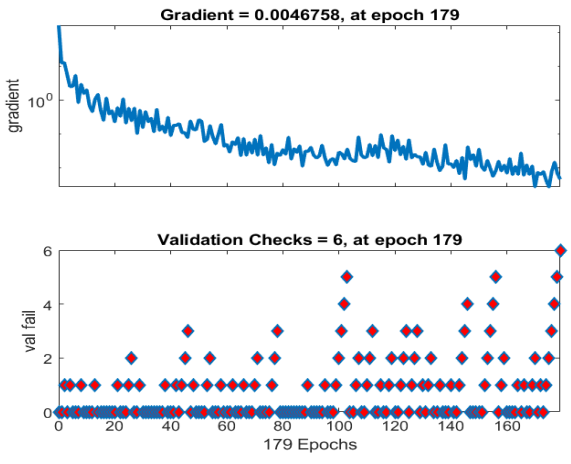

(d) TS for case 1

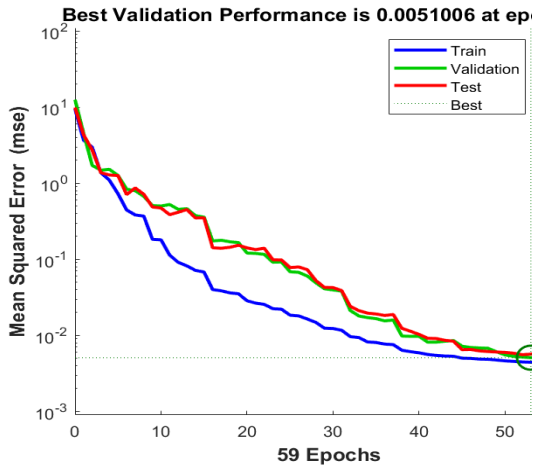

(b) Optimal training (2)

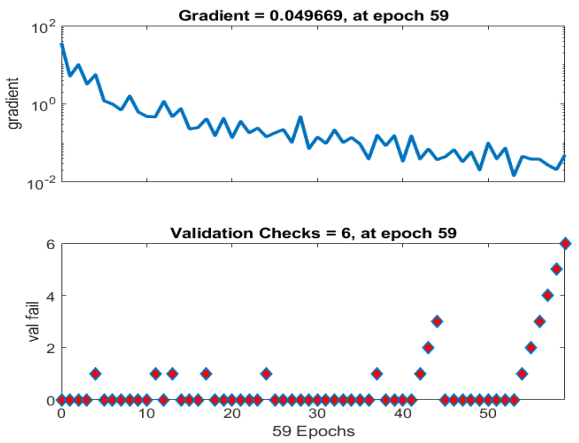

(e) TS for case 2

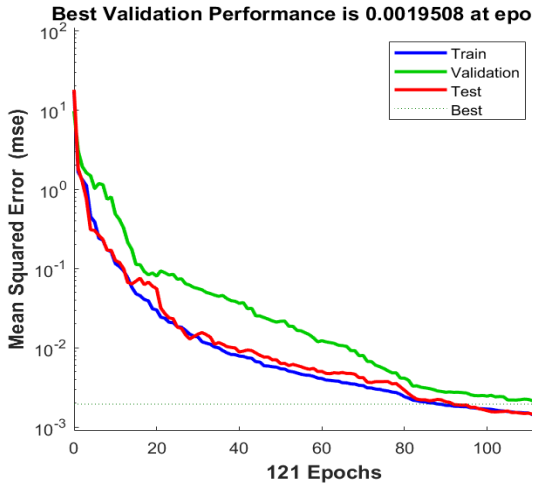

(c) Optimal training (3)

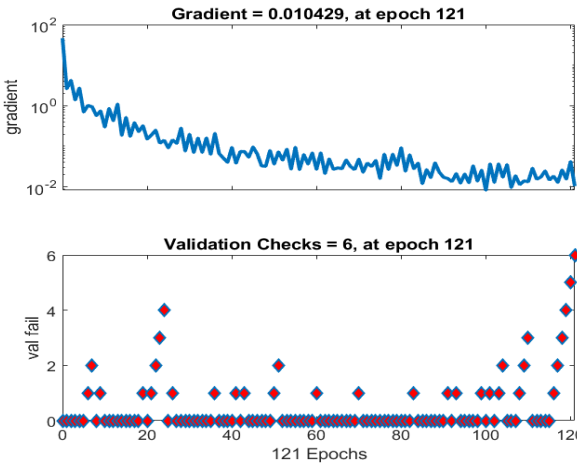

(f) TS for case 3

Figure 3. Best training and TS for the FO-LSDM

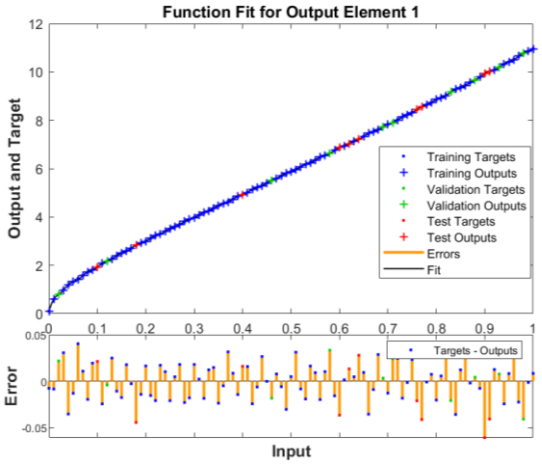

(a) function fit for case 1

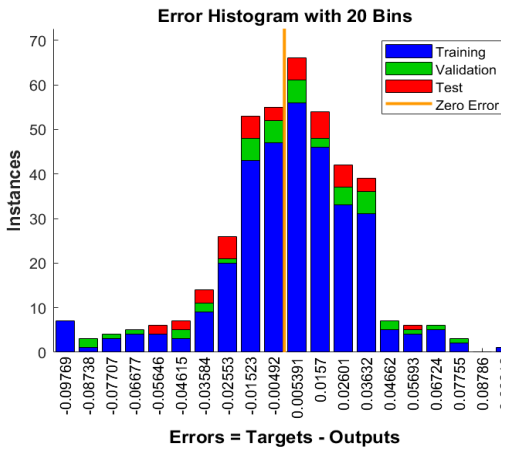

(d) EH (1)

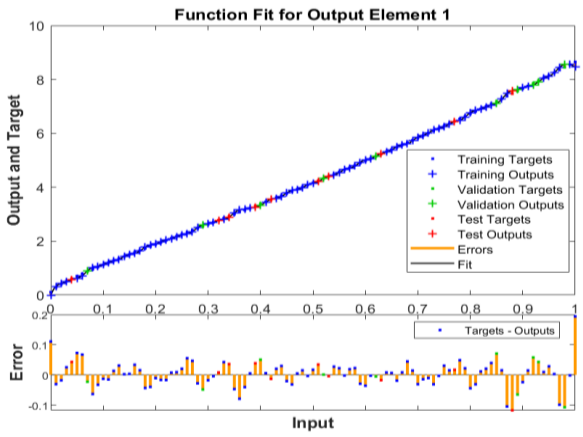

(b) function fit for case 2

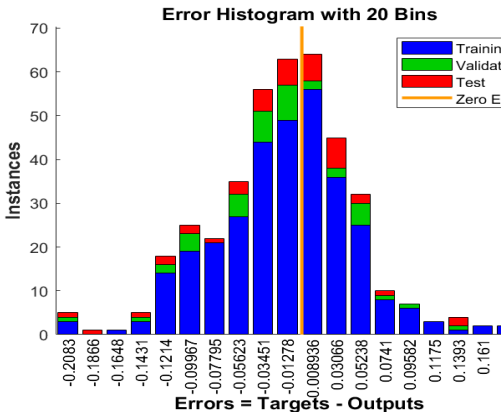

(e) EH (2)

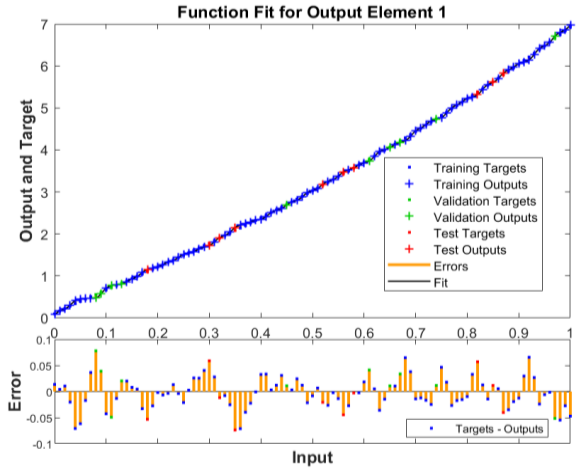

(c) function fit for case 3

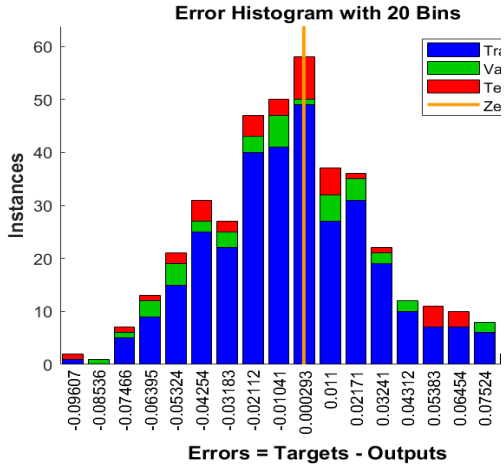

(f) EH (3)

Figure 4. Function fit and EH for the FO-LSDM

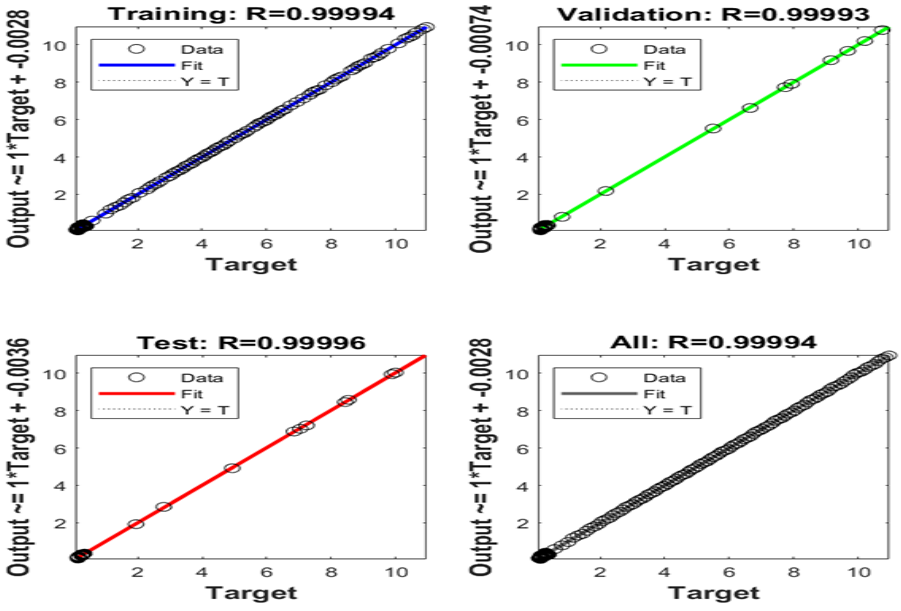

Figure 5. Regression values for the FO-LSDM (1)

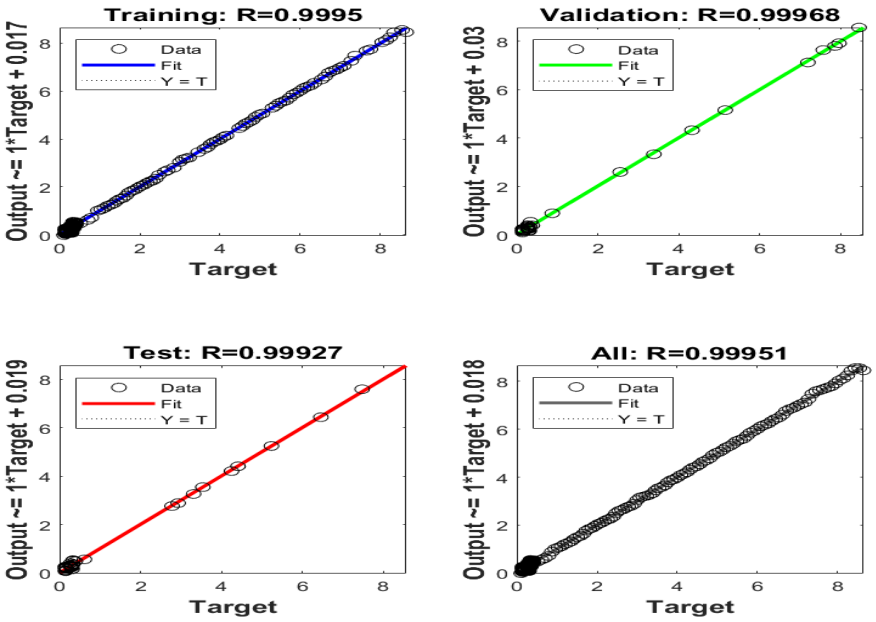

Figure 6. Regression values for the FO-LSDM (2)

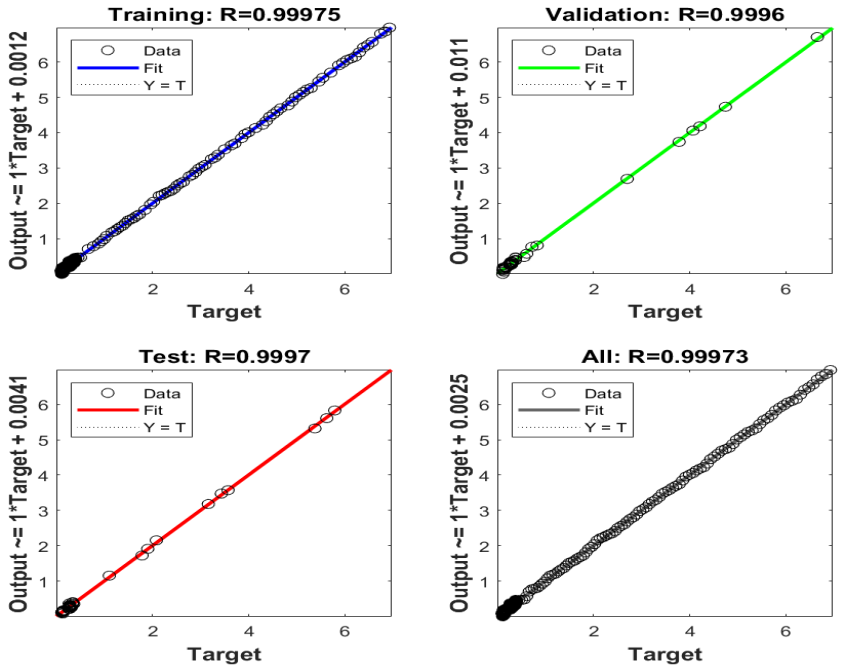

Figure 7. Regression values for the FO-LSDM (3)

Figs. 8 and 9 represent the outcomes matching and values of the AE for the FO-LSDM using the structure of ANN along with the optimization of SCGD. Fig. 8 presents shows the scheme's accurateness, which is performed through the matching of each class of the FO-LSDM. Fig. 9 indicates the outputs related to the AE based on the FO-LSDM. The AE values are reported around 10^{-04} to 10^{-06} for each scenario of the FO-LSDM, which shows that these insignificant AE perform the correctness of the ANN structure along with the optimization of SCGD.

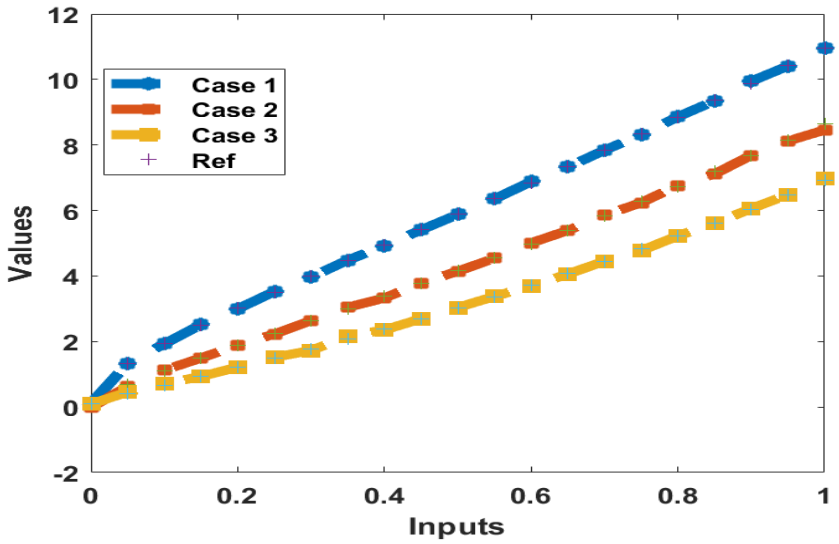

(a) Outcomes for the category *Sc*(*u*)

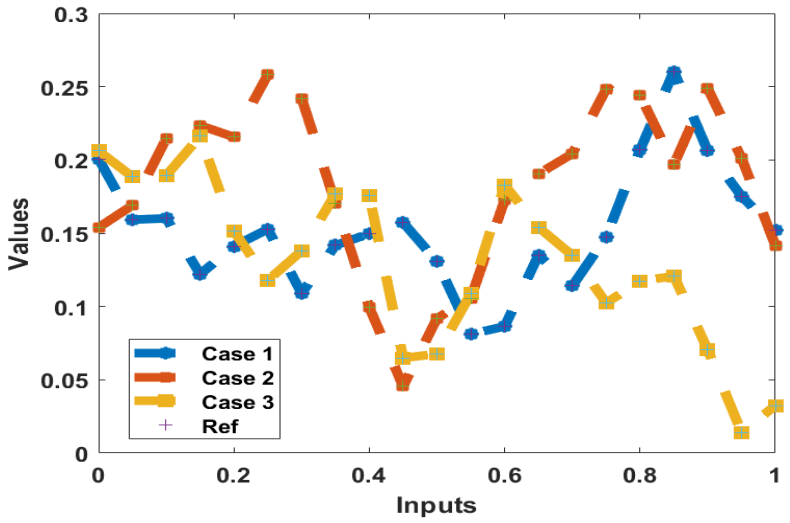

(b) Outcomes for the category *Ic*(*u*)

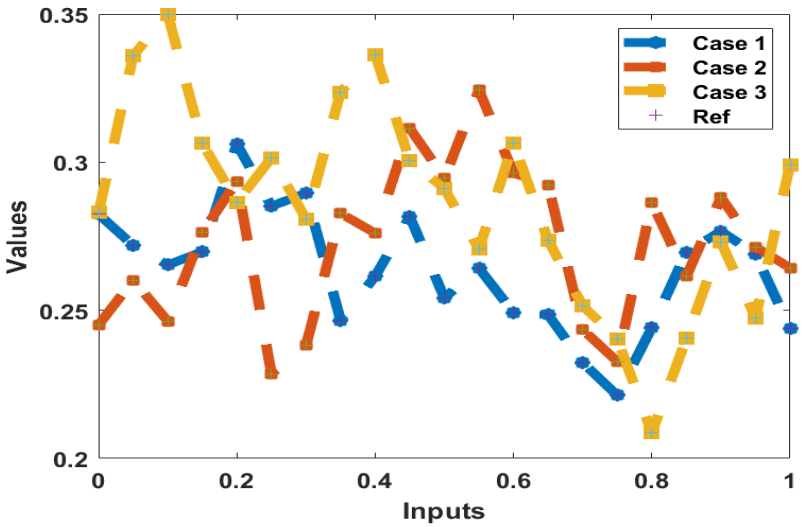

(c) Outcomes for the category *Sv*(*u*)

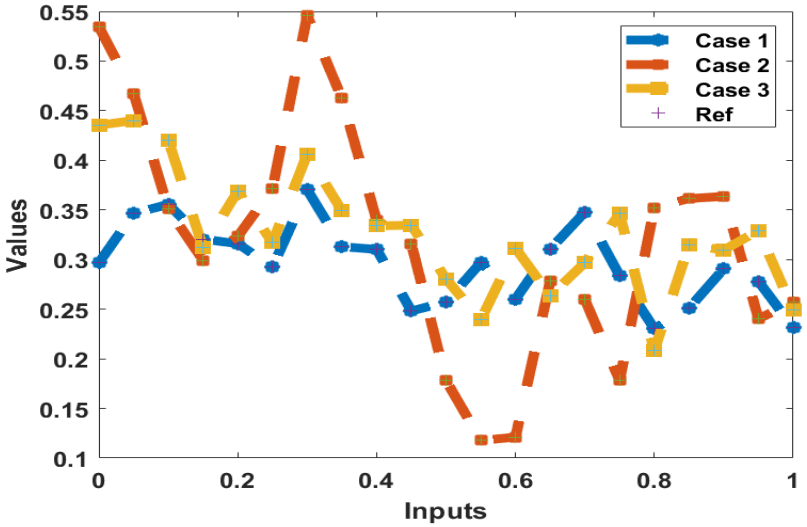

(d) Outcomes for the category $Iv(u)$

Figure 8. Result performances for each case of the FO-LSDM

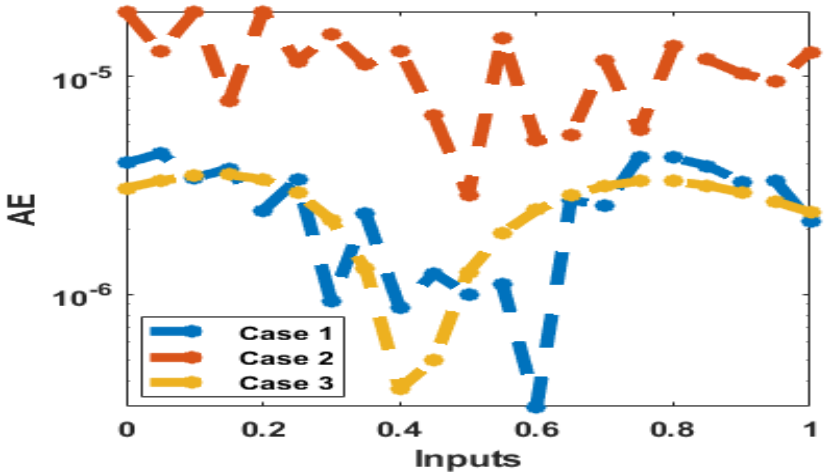

(a) AE illustrations for the category $Sc(u)$

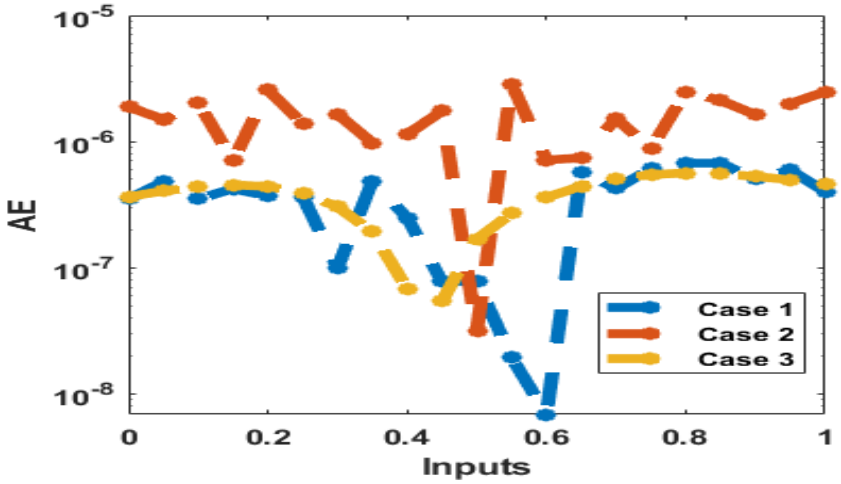

(b) AE illustrations for the category $Ic(u)$

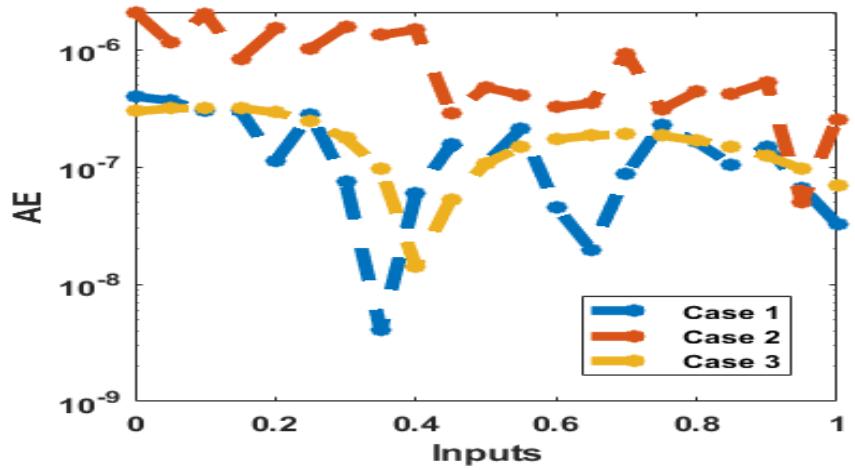

(c) AE illustrations for the category $Sv(u)$

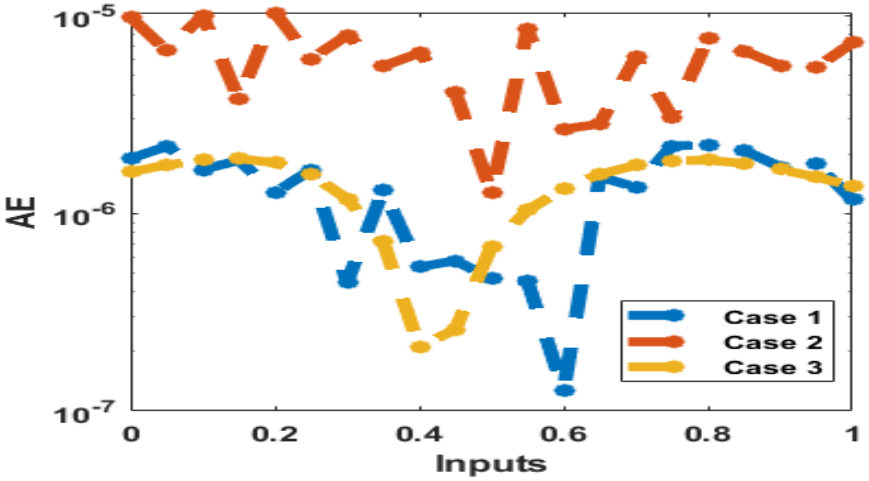

(d) AE illustrations for the category $Iv(u)$

Figure 9. AE representations for each scenario of the FO-LSDM

4. Conclusion

In this study, a computational artificial neural network design has been presented for the numerical outcomes of the fractional order lumpy skin disease model. The stochastic performances using the optimization of scale conjugate gradient have been implemented to get the solutions of the model. The mathematical LSDM is divided into two populations based on the cattle and vector using the population of susceptible and infected. Some of the conclusions of this study are presented as:

- The stochastic performances based on the ANN along with the optimization of SCGD have been implemented to achieve the numerical solutions of the system.
- The implementation of the FO results has been considered more reliable as compared to the integer order.
- An operator based on the Caputo FO derivative has been used between 0 and 1 for solving the model.
- A numerical Adam scheme has been accomplished to find the dataset in order to reduce the MSE by splitting the statics of endorsement, testing and training as 13%, 12% and 75%.
- A single layer has been used in the neural network procedure, which is taken as a sigmoid activation function.
- Thirty numbers of neurons have been taken together with the optimization of SCGD procedure.
- The exactitude of the SCGD neural network has been authenticated through the result comparisons and reducible absolute error around 10^{-06} to 10^{-08}.
- The correctness of the stochastic process using the SCGD neural network has been assessed by applying different stochastic procedure.

Acknowledgement: The author would like to thank the editor and anonymous reviewers for their comments that help improve the quality of this work.

Funding Statement: I would like to acknowledge the initial support received from Jadara University under grant number Jadara-SR-Full2023. This support played a vital role in facilitating this research.

Availability of Data and Materials: The author confirm that the data supporting the findings of this study is available within the article.

Conflicts of Interest: The author declare that they have no conflicts of interest to report regarding the present study.

References

[1] R. I. Abdulganiy et al., "A functionally-fitted block hybrid Falkner method for Kepler equations and related problems," *Computational and Applied Mathematics*, vol. 42, no. 8, p. 327, 2023. DOI: 10.1007/s40314-023-02463-y.

[2] I. Onder et al., "Stochastic optical solitons of the perturbed nonlinear Schrödinger equation with Kerr law via Ito calculus," *The European Physical Journal Plus*, vol. 138, no. 9, p. 872, 2023. DOI: 10.1140/epjp/s13360-023-04497-x.

[3] M. Alquran et al., "Novel investigations of dual-wave solutions to the Kadomtsev–Petviashvili model involving second-order temporal and spatial–temporal dispersion terms," *Partial Differential Equations in Applied Mathematics*, vol. 8, p. 100543, 2023. DOI: 10.1016/j.padiff.2023.100543.

[4] S. Qureshi et al., "A new optimal root-finding iterative algorithm: local and semilocal analysis with polynomiography," *Numerical Algorithms*, vol. 95, no. 4, pp. 1715-1745, 2024. DOI: 10.1007/s11075-023-01625-7.

[5] W. Adel et al., "Investigating the dynamics of a novel fractional-order monkeypox epidemic model with optimal control," *Alexandria Engineering Journal*, vol. 73, pp. 519-542, 2023. DOI: 10.1016/j.aej.2023.04.051.

[6] H. Joshi et al., "Stability analysis of a non-singular fractional-order COVID-19 model with nonlinear incidence and treatment rate," *Physica Scripta*, vol. 98, no. 4, p. 045216, 2023. DOI: 10.1088/1402-4896/acbe7a.

[7] H. Joshi et al., "Modelling and analysis of fractional-order vaccination model for control of COVID-19 outbreak using real data," *Mathematical Biosciences and Engineering*, vol. 20, no. 1, pp. 213-240, 2023. DOI: 10.3934/mbe.2023010.

[8] M. Higazy et al., "Numerical, approximate solutions, and optimal control on the deathly lassa hemorrhagic fever disease in pregnant women," *Journal of Function Spaces*, vol. 2021, pp. 1-15, 2021. DOI: 10.1155/2021/2444920.

[9] H. R. Pandey et al., "Vaccination effect on the dynamics of dengue disease transmission models in Nepal: A fractional derivative approach," *Partial Differential Equations in Applied Mathematics*, vol. 7, p. 100476, 2023. DOI: 10.1016/j.padiff.2022.100476.

[10] M. Yavuz et al., "A new mathematical model for tuberculosis epidemic under the consciousness effect," *Mathematical Modelling and Control*, vol. 3, no. 2, pp. 88-103, 2023. DOI: 10.3934/mmc.2023009.

[11] W. Ahmad et al., "Effect of quarantine on transmission dynamics of Ebola virus epidemic: a mathematical analysis," *The European Physical Journal Plus*, vol. 136, no. 4, pp. 1-33, 2021. DOI: 10.1140/epjp/s13360-021-01360-9.

[12] A. Elsonbaty et al., "Dynamical analysis of a novel discrete fractional lumpy skin disease model," *Partial Differential Equations in Applied Mathematics*, vol. 9, p. 100604, 2024. DOI: 10.1016/j.padiff.2023.100604.

[13] A. S. Heilat et al., "Hybrid Cubic B-spline Method for Solving A Class of Singular Boundary Value Problems," *European Journal of Pure and Applied Mathematics*, vol. 16, no. 2, pp. 751-762, 2023. DOI: 10.29020/nybg.ejpam.v16i2.4725.

[14] A. Al-Husban et al., "A new incommensurate fractional-order COVID-19: modelling and dynamical analysis," *Mathematics*, vol. 11, no. 3, p. 555, 2023. DOI: 10.3390/math11030555.

[15] A. Hioual et al., "Fractional discrete neural networks with variable order: solvability, finite time stability and synchronization," *Eur. Phys. J. Spec. Top.*, 2024. DOI: 10.1140/epjs/s11734-024-01167-6.

[16] T. Hamadneh et al., "The FitzHugh–Nagumo Model Described by Fractional Difference Equations: Stability and Numerical Simulation," *Axioms*, vol. 12, no. 9, p. 806, 2023. DOI: 10.3390/axioms12090806.

[17] T. Hamadneh et al., "Fast Computation of Polynomial Data Points Over Simplicial Face Values," *Journal of Information & Knowledge Management*, vol. 19, no. 01, 2040001, 2020. DOI: 10.1142/S0219649220400018.

[18] A. S. Heilat et al., "The new fractional discrete neural network model under electromagnetic radiation: Chaos, control and synchronization," *Alexandria Engineering Journal*, vol. 76, pp. 391-409, 2023. DOI: 10.1016/j.aej.2023.06.017.